Process Engineering of Semi-transparent DSSC Modules and Panel Incorporating an Organic Sensitizer

Luigi Vesce, Paolo Mariani, Massimo Calamante, Alessio Dessì, Alessandro Mordini, Lorenzo Zani, and Aldo Di Carlo**

Dr. L. Vesce, Dr. P. Mariani, Prof. A. Di Carlo
CHOSE – Centre for Hybrid and Organic Solar Energy, Department of Electronic Engineering, University of Rome "Tor Vergata", Via del Politecnico 1, 00133 Rome – Italy
E-mail: aldo.dicarlo@uniroma2.it

Dr. M. Calamante, Dr. A. Dessì, Dr. A. Mordini, Dr. L. Zani
Institute of Chemistry of Organometallic Compounds (CNR-ICCOM), Via Madonna del Piano 10, 50019 Sesto Fiorentino - Italy
E-mail: lorenzo.zani@iccom.cnr.it

Dr. M. Calamante, Dr. A. Mordini
Department of Chemistry "U. Schiff", University of Florence, Via della Lastruccia 13, 50019 Sesto Fiorentino - Italy

Prof. A. Di Carlo
Institute of Structure of Matter (CNR-ISM), via del Fosso del Cavaliere 100, 00133 Rome - Italy

Keywords: Dye sensitized solar cell, PV module, PV panel, stability studies, semi-transparent, BIPV.

Abstract

Among the photovoltaic technologies adopted in the building-integrated photovoltaics (BIPV) sector, Dye-Sensitized Solar Cells (DSSCs) appear very attractive because of unique features like tunable color and good transparency. However, the prospect of their low-cost fabrication is realistic only if reliable and scalable processes under real manufacturing conditions (*i.e.* pilot line and/or plant factory) are designed, developed and optimized for large-area, efficient and stable devices. Here, we show a highly reproducible process based on the deposition of different inks by screen-printing technique to realize twenty modules (400 cm^2) and one panel (0.2 m^2) incorporating an organic sensitizer. Module design considers the resistive losses caused by the electron transport, the durability of the device and the aspect ratio (more than 70%). The module champion efficiency was 5.1% with 35.7% transparency (AVT - Average Visible Transmittance), and its stability (ISOS-D-2 and ISOS-L-1) was determined to be >1000 h. The modules showed no structural failures, electrolyte leakage, grids corrosion, empty liquid electrolyte zones and moiré patterns on the sealing part. The consistency of the gap between photo- and counter-electrode before and after the stress was demonstrated. An industrial lamination process to realize a panel with an outdoor efficiency of 2.7% at 60 °C tilt angle was adopted.

1. Introduction

Dye Sensitized Solar Cells (DSSC) have been the first third-generation photovoltaic (PV) technology developed to commercialization level [1–4]. Although device efficiency (PCE, power conversion efficiency) is still low (13% for small area cells and 8.8% for sub-modules) if compared to the well-known silicon-based technology (more than 26%) [5,6], some peculiar features make DSSCs very attractive for building-integrated photovoltaics (BIPVs) [7–10], such as: control of device color [11], transparency in the visible range [12,13], low dependence of performance on the light angle [14,15], better response in diffuse light compared to semiconductors-based PV technologies [16] and environmental sustainability [17]. BIPV market is expected to grow by 150% in the next decades as a result, among others, of the renewable energy integration policies of the European Union [17,18]. In this regard, buildings equipped with BIPV devices could be viewed like small and distributed power plants with annual near-zero energy balance [19,20]. Accordingly, modules and panels must be highly transparent (transmittance range between 25% ad 38%) and efficient, to act as glazing building envelopes, curtain-wall façades or large skylights [21–25]. Among PV technologies applicable to building integration, c-Si has very high efficiency and the mutual distance between individual cells can be settled to have some transparency, but the pattern produces shades not comfortable for the internal living [19,22]. Besides, tilt angle and low irradiation levels complicate their integration in architectural glazing.

In DSSC technology, the TiO_2 thickness and adopted dye molecule play a key-role to define the optical properties of the device [4,26–28]. In particular, the chosen dye must present some essential features [29], including: absorption spectrum covering the whole visible region, presence of appropriate anchoring groups for binding to the semiconductor surface, correct energy level alignment with both the semiconductor and the redox mediator, sufficient chemical and photo-stability. The superposition of electrolyte and dye spectra is responsible of the DSSC color, while TCO (transparent conductive oxide), dye, electrolyte, platinum (counter electrode material), and TiO_2 particle size and thickness all influence the transparency of the device (e.g. small particle size and low thickness give high transparency, but the corresponding devices usually present a lower current density respect to high thickness or scattering layer based cells) [9,13,30–33]. Semi-transparent DSSC based on dyes with symmetrical NIR-selective heptamethyne cyanine and donor-π-conjugated-bridge-acceptor (D-π-A) structure got efficiencies of 3.1% and 4.17%, respectively [34,35].

The industrialization and commercialization of DSSC technology is feasible if different cells are connected to realize a Dye Sensitized Solar Module (DSSM) [4]. This complicates the

manufacturing, performance and stability respect to lab cells. The TCO glass substrates limit the performance of DSSMs, because of non-negligible sheet resistance (6-10 ohm/sq) that can induce large ohmic losses when the current of the cell increases [3]. This issue is overcome by depositing conducting grids onto the conductive substrates [36] or by realizing modules with narrow cells connected in series (monolithic, W, Z) or parallel/monolithic [4,16,37–41]. A layout and interconnection optimization process is thus needed to find the best suitable single cell width according to illumination, sheet resistance, fabrication technology, efficiency and durability [41–43]. Finally, sealing of the individual cells in modules is critical, since any sealant failure can severely limit the module lifetime [44].

In this context, the scaling up from small lab cells to modules and panels by adopting simple and low cost fabrication processes is of paramount importance, as for other third generation PV technologies [3,22,45,46]. DSSMs and panels (DSSPs) can be fabricated by methods inherited from other industrial sectors and the manufacturing process should achieve a reliable/high throughput production, good performance and stability [16,47,48]. In any case, most of the procedure details are hidden because of the industrial relevance of the upscaling process. In the last decades, some examples of semi-transparent DSSMs have been reported. Sastrawan *et al.* reported a 900 cm^2 meander-shaped semi-transparent module with an efficiency of 3.1% [42]. Takeda *et al.* showed a transparent monolithic serial-connected device (9.5×9.5 cm^2) by using Pt-loaded In_2O_3:Sn nanoparticles and an insulator composed of SiO_2 particles [49]. In 2014, Solaronix installed 300 m^2 of DSSPs (W-connected modules) on Swiss Tech Convention Center façade at EPFL campus [50]. The single module was 35×50 cm^2 with 1.05% efficiency based on active area. Despite the impressive installation, many modules appeared degraded by different routes [4]. Vesce *et al.* showed a series of Z-connected 600 cm^2 module fabricated in the Italian Dyepower pilot line facility with Dyenamo D35 dye [3,4,17]. The efficiency and the transparency were 5.6% and 30%, respectively. The devices underwent UV pre-conditioning, humidity freeze and damp heat tests (IEC 61215). Moreover, the environmental profile was compared to other PV technologies [17]. H.Glass and Dongjin Semichem realized huge DSSC installations on Science Tower in Austria and on Roskilde University in Denmark, respectively [4]. Lee *et al.* tested a semi-transparent, series connected 900 cm^2 module from a Korean company with an efficiency of 2.76% [51]. Kim *et al.* reported Z-type 900 cm^2 module with Z907 dye and 3.19% efficiency [52]. Godfroy *et al.* showed a 23 cm^2 semi-transparent module (W-type connection) with 8.7% efficiency based on active area and 26% AVT (Average Visible Transmittance) by adopting a benzothiadiazole-based photosensitizer [53]. According to this short overview, just in two cases the AVT [3,17,53] values have been reported (no data about the color rendering index – CRI) and no specific details about the fabrication

procedure and the aspect ratio of the devices were provided. Moreover, in agreement with the observations of Muñoz-Garcia *et al.* [4], we found a lack of published stability tests of semi-transparent modules.

In this paper, we show the detailed fabrication procedure of twenty semi-transparent DSSMs (400 cm^2 each) with high reproducibility, and of one DSSP (0.2 m^2), all containing the dye TTZ5, a thiazolo[5,4-*d*]thiazole (TzTz) organic sensitizer with strong visible light absorption [54]. Modules are designed by considering the trade-off between low losses and device sturdiness. The finest module has an efficiency of 5.1% on active area (70% aspect ratio) and a transparency of 35.7% on aperture area (315.4 cm^2) that is appropriate for BIPV application [23]. According to ISOS-D-2 and ISOS-L-1 standard tests, the modules are stable for more than 1000 h at 85 °C and under light soaking without any electrolyte leakage, collectors corrosion or delamination. Nine modules are assembled in three strings and then in one laminated panel by an industrially-compatible process. The maximum efficiency of the panel under outdoor illumination conditions at 60° tilt angle is 2.7%.

2. Results and Discussion

2.1 Choice of the organic dye and synthesis

Compared to typical metalorganic sensitizers, such as Ru-bipyridine complexes, organic dyes present some potential advantages in the context of BIPV applications, such as: the simple and scalable synthetic routes, the absence of any heavy, toxic or critical metal (whose supply could be limited in the case of large-scale module production), the high molar attenuation coefficients in the visible region and the possibility to easily tune their electronic properties by precise structural modifications, making several color nuances accessible starting from the same general structure [4].
In this regard, dye TTZ5, reported for the first time by some of us in 2014, stood out for its broad light absorption in the visible region (λ_{max} = 487 nm and λ_{onset} > 650 nm on TiO_2) and its above-average molar attenuation coefficient ($\varepsilon = 9.41\times10^4$ M^{-1} cm^{-1}, measured in THF solution), properties that made it a very suitable candidate as a photosensitizer for semi-transparent thin-film DSSCs [55]. Small-scale DSSCs (active area = 0.25 cm^2) containing a semi-transparent 5.5 μm-thick TiO_2 layer photosensitized with TTZ5 and HPE (High Performance Electrolyte, Great Cell Solar) electrolyte, showed a remarkable light-to-energy conversion efficiency of 7.39% (FF = 63%), without the need of any coadsorbent, such as chenodeoxycholic acid (CDCA), outperforming a standard organic dye (D5) and the Ru-based sensitizer Z907. Dye TTZ5 confirmed its excellent

photovoltaic performances (PCE = 6.20–6.35%, FF = 53%) in larger area cells (active area: 3.6 cm^2) with even smaller TiO_2 thicknesses (3–5 μm). Cells built with HSE (High Stability Electrolyte, Great Cell Solar) electrolyte showed excellent stability, steadily around 6%, over a period of 1000 h, during which they were stored in the dark at 85 °C [54]. It is noteworthy that these results were obtained keeping device fabrications as simple as possible, without any TiO_2 blocking layer and light-scattering layer, and employing a commercial electrolyte solution containing the simplest redox couple, I^-/I_3^-. For these reasons, TTZ5 appeared a promising candidate dye for larger-scale BIPV applications.

Recently, we completely revised the synthesis of TTZ5 [56]. to achieve a gram-scale preparation of the dye, reduce the amount of waste produced and its cost, and shorten the number of synthetic steps in comparison to the original synthesis (Figure S1) [55]. Following the reported procedure (see Supporting Information), we were able to prepare TTZ5 dye on gram-scale, enough for the fabrication of the modules and panel described in the following paragraph.

2.2 Fabrication of dye sensitized solar modules and panel

Device performances are limited by sheet resistance of the transparent conductive substrates when scaling up from lab cell to module. The resistive losses are mitigated by patterning the substrate in several interconnected cells [3]. Among the different module architectures (parallel, series monolithic, series W-type and series Z-type connection), we adopted the series Z-type connection due to the high voltage of the resulting device, as well as the uniform and reliable power output over large area in different illumination and temperature conditions [57]. Conversely, the parallel connection has a low working potential and high output current that leads to high power losses, while W-type connection suffers of imbalanced cells (mainly concerning the photocurrents), since half of them receives sunlight from the counter-electrode side [40]. In the series Z-type connection, the charge collection from the cells and the electrical connections are guaranteed by a conducting material placed between the sandwiched conductive substrates. Conductors and cells must be effectively insulated to avoid metal corrosion and unwanted mass transport between the cells, respectively [16,58]. The presence of spikes in the metal conductor, or the volume expansion of the electrolyte, could affect the device sealing, pushing the electrodes away from each other with a subsequent electrolyte leakage [59,60]. The vertical connections and sealant can also cause some troubles during the assembling process of the modules, since tolerances for their height variations are usually tight [3]. The best interconnection strategy to fabricate efficient and stable Z-type DSSC modules according to ISOS (International Summit on Organic Photovoltaic Stability) and IEC

(International Electrotechnical Commission) standards is still an open technological issue [60–62]. Few works showed the possibility to mitigate the aggressive action of the electrolyte by using grids of metals different than silver, such as nickel, chromium, tungsten and molybdenum in form of wires, or protecting silver by adopting processes different from printing [63–66]. Hopkins *et al.* adopted a Ti-based compound composed by 45 μm Ti particles and 5 μm W particles in a polymer matrix [67]. Since the compound was less sensitive to electrolyte corrosion compared to Ag, a new design without protection for the grids could be used. However, the resulting vertical connections were less conductive than those based on Ag, causing a reduction of module efficiency. Tulloch *et al.* protected the metallic conductors from the tri-iodide/iodide couple by applying chemically inert nonmetallic materials, such as TiN, ZrN or boron carbide [68]. The manufacturing complexity was increased, and the module lost the bifacial feature to be illuminated from photo- and counter-electrode [69,70]. Recently, we showed how graphene can act as a collector in DSSM [60]. In that case, we increased the number and the width of the cells in the substrate, but the contact resistance between FTO and graphene was still high.

We designed the device according to the equivalent circuit models of DSSC and DSSM developed on the electronic simulation software Orcad PSpice, as reported in a recent publication [3]. To evaluate the optimized layout of a Z-type connection, we used the single cell electrical parameters from previous published works by our groups that adopted the same materials reported in the experimental section [54,71]. The module dimensions, including single cell area, conductors' width, inter-distance between two adjacent cells and aspect ratio are reported in Table 1 and Figure 1. The layout also considers the space for a robust sealing all around the aperture area and the conductors.

Table 1. Device geometrical details. Parameters defined as in ref.[3].

Module size (cm^2)	20×20
Substrate size (cm^2)	19.2×20
Number of cells	12
Single cell active area (cm^2)	18.5 (10.25 mm × 180.5 mm)
Module active area (cm^2)	222
Aperture area (cm^2)	315.4
Aspect ratio (%)	70.4
Inter-distance (mm)	4.7
Conductor width (mm)	1

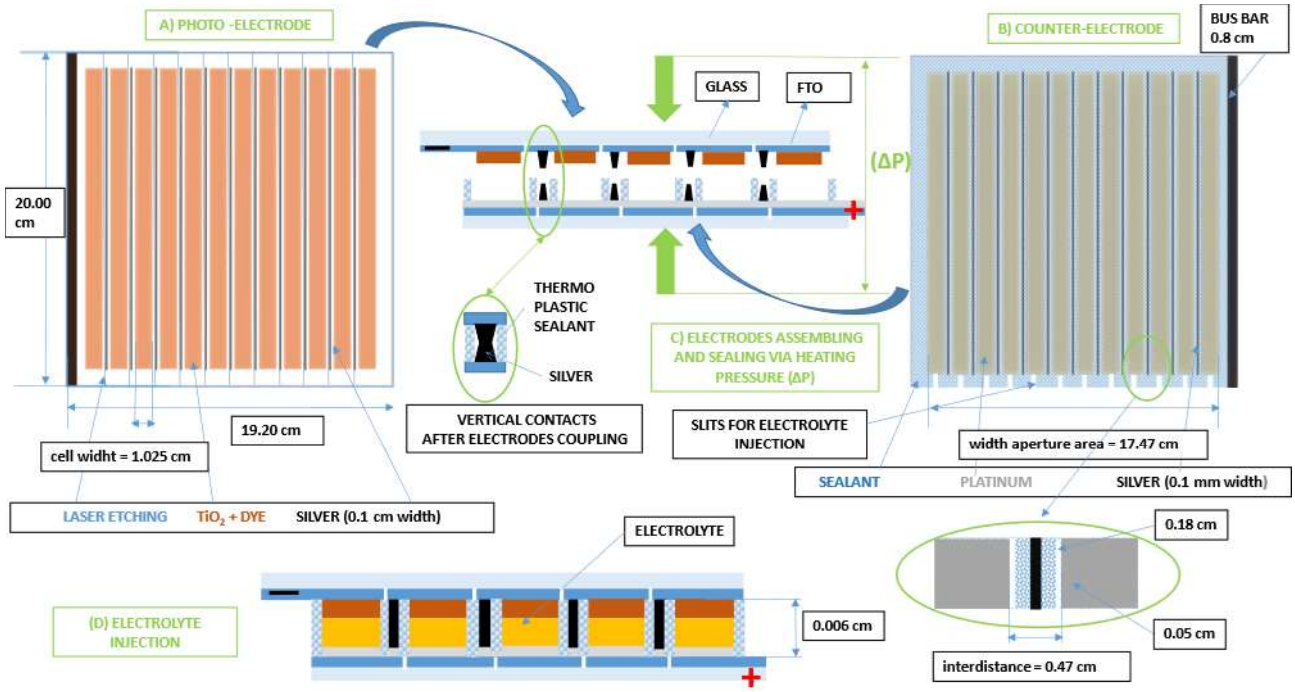

Figure 1. DSSMs layout and series Z-type connection. A) Photo-electrode (laser scribes in sky blue, TiO_2 + dye in brown, silver in black); B) Counter-electrode (platinum in grey, thermoplastic sealant in textured blue); C) The two electrodes just before the coupling; D) The two electrodes after the assembling with the injected electrolyte (in yellow).

The manufacturing process of 20 modules is depicted in Figure 2 and the details are reported in the Experimental Section. Each module is composed by two FTO (fluorinated tin oxide)-covered glass sheets (2.2 mm thick), one for the photo-electrode (PE) and one for the counter-electrode (CE). The laser scribing step was used to insulate adjacent cells by removing a narrow line of FTO [72] (Figure 2,a). The next steps highlighted the advantage of DSSC technology by employing the well-known, high throughput and cheap screen-printing technique to deposit silver conductors and bus bars on both electrodes, TiO_2 film on PEs and Pt clusters on CEs [3,58] (Figure 2,b). The homogeneity of each of these materials is mandatory to ensure that all cells in the module have comparable performances. The first printed material was a low-resistivity conductive silver paste for external bus bars and collecting/interconnection grids. The latter collect charges produced by each single cell and connect it to the next cell. The width of the conductors was optimized according to the trade-off between the highest possible active area, sufficient space for sealant and maximum power output [3]. Electrodes were fired at 120 °C for 30 min to dry the ink before the deposition of TiO_2 and Pt pastes. The PEs (Ag + TiO_2) were sintered at 500 °C for 30 min (2.5 h ramping) and the CEs (Ag + Pt) were fired at 480 °C for 30 min (2 h ramping), obtaining a thickness of 31 µm and 5.5 µm for

Ag grids and TiO_2 layer, respectively. In both cases, the thermal process was optimized to avoid any glass deformation that can have detrimental effects on the reliability of the devices [59]. The sintering process of the PE is necessary to strengthen the electrochemical bonds between TiO_2 nanoparticles and to burn organic solvents and binders present in the paste [13,73]. The firing step of the CE permits to thermally reduce the Pt precursor-based paste to the elementary form of the metal [72,74]. During the dipping step (15 h), the nanocrystalline semiconductor films adsorbed a large amount of the organic TTZ5 dye molecules, increasing the harvesting efficiency of solar energy [71] (Figure 2,c). Since the PEs sensitization step is the bottleneck of the process [17], dye drops can be generated on demand by an ink jet printer, avoiding waste and reducing material consumption [75].

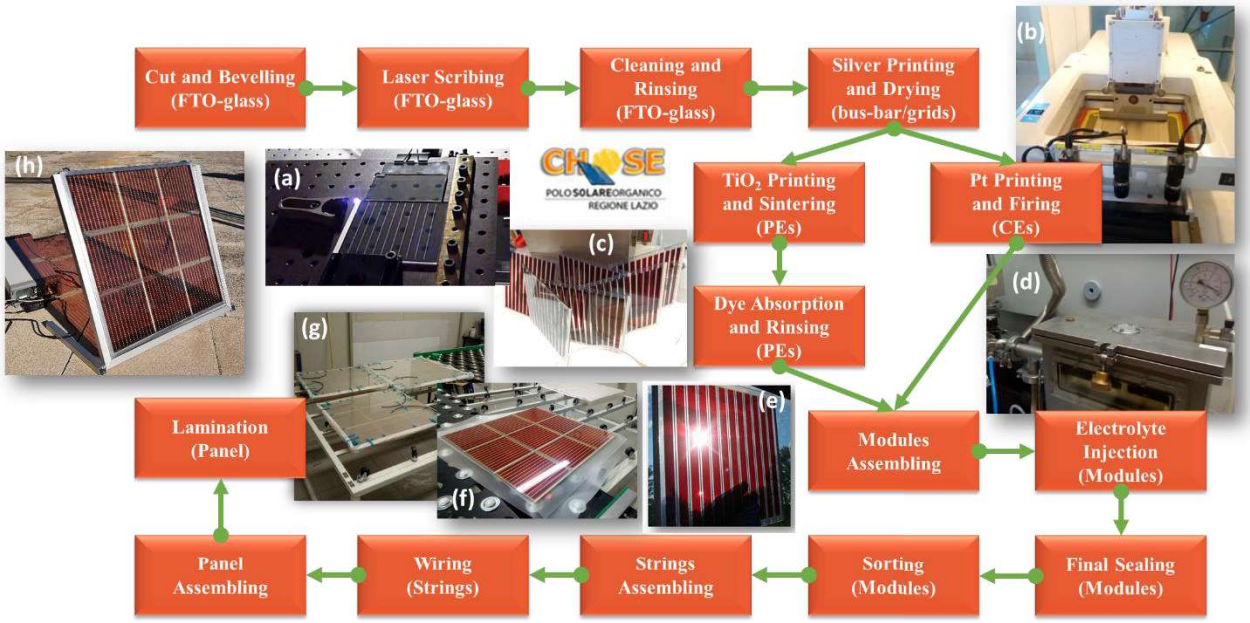

Figure 2. Process flow for DSSMs e DSSP fabrication. The full process is in ambient environment. (a) FTO-glass laser scribing; (b) ink screen-printing; (c) dye sensitized PEs; (d) electrolyte injection chamber; (e) DSSM; (f) panel assembling; (g) panel pre-lamination stage; (h) DSSP.

In the assembling step, the PE and the CE were coupled and pressed together with a printing press system. A thermoplastic sealant was added at the interface of the substrates to avoid electrolyte leakage (possibly causing corrosion of the metal contacts) and solvent evaporation. The process was composed of four steps: 1) Bynel™ thermoplastic foil cutting according to active areas, grids, bus bar, electrolyte injection slits and substrate edges; 2) positioning of the foil on the CE and pressing under high temperature; 3) alignment of PE and CE and pressing under high temperature till thermoplastic melting; 4) slits sealing by pressure and temperature after electrolyte injection. In the first step, a small slit was shaped for the subsequent electrolyte injection process (Figure 1). Since the slit must be kept open until the third step, precise control of temperature and pressure

parameters in the following step is mandatory. Indeed, during the second step, the thermoplastic foil must stick on CE without melting, as instead necessary in the third step, in which the two electrodes were sealed together and aligned to series connect the grids (Figure 1), and the thermoplastic foil became transparent after melting. In the fourth step, only the edge of the module with the slits was positioned under the pressure system to avoid thermal and pressure overexposure of the polymer in the main part of the device.

The surface occupied by the thermoplastic gasket is designed to avoid any overlapping with cells and conductors (Figure 1). Moreover, the thickness of the sealant defines the electrodes gap and was adjusted to withstand thermal expansion of the liquid electrolytes and substrates traction. In detail, the thicknesses of the thermoplastic foil and of the silver conductor on one electrode are 80 µm (about 60 µm after the assembling process, *i.e.* the spacing of the electrodes) and about 30 µm, respectively. The designed and obtained thicknesses were optimized to guarantee the electrical series interconnection and uniform gaps between PE and CE for each cell in the module. According to literature reports, assembling modules with cells wider than 18 mm was required to obtain uniform thickness of the internal module gap and thermal reliability [52,76]. In our work, we obtained both a homogeneous gap (before and after the thermal stress, Figure S2) and stable module devices (see below, Section 2.4) with a cell width of 10.25 mm. We report the gap/thickness values in 9 distributed points of a dummy module before and after the thermal stress (Figure S2). The dummy module experienced all the process steps and relative stresses (thermal and mechanical) of the working modules except for the dye dipping and Pt deposition, to make the measurement possible (see Experimental Section). In Figure S2, it's easy to appreciate the high homogeneity (59 ± 2 µm) and the consistency of the gap after a thermal stress at 85 °C for more than 1000 h (only approx. 1 µm average difference compared to the initial value). Sealing of the device is mandatory to prevent electrolyte leakage, evaporation of solvents and delamination of the substrates (i.e. substrates traction and thermal expansion) [77,78]. In the case of a DSSM, the sealant must mainly protect the conductors from the corrosive action of the liquid electrolyte. Here, the width dedicated to the protection of the conductor was equal to 3.6 mm (1.8 mm on both sides of the conductor). The next fabrication step was the electrolyte injection by the vacuum backfilling technique through the pre-cut slits (Figure 1) in the sealing gasket [79]. To this end, a specially designed vacuum chamber (Figure 2,d) was employed, which allows simultaneous filling of ten modules, placed in vertical position.

The fabricated modules were assembled/laminated in strings and panels to protect all components from environment contamination, and to guarantee sturdiness and longevity of the devices [3]

(Figure 2 and Figure S3). The lamination process must not take place above a temperature of 90–100 °C to avoid degradation effects on dye, electrolyte and sealant. Three modules were connected in series by overlapping the bus bars to realize a string. Three strings were then connected in parallel with a conductive tin ribbon soldered on the bus bars. Before the lamination process, two cables were applied on the positive and negative contact of the panel. For the lamination, the panel (total surface 59 × 61 cm^2) was sandwiched in between two 4 mm-thick tempered glass sheets, and two 1.52 mm-thick PVB (polyvinyl butyral) foils. The glass/PVB/Panel/PVB/glass stack was inserted in a silicon bag under vacuum and then in an autoclave (10 m^2/h throughput) at controlled pressure and temperature for 2 h, according to a procedure adopted in architectural, automotive, and ballistic applications. PVB guarantees strong binding, optical clarity, toughness, adhesion and adaptation to devices and irregularity of the surface, but it is generally cured at temperatures above 150 °C at more than 5 bar. Therefore, a lengthy optimization of the process parameters (pressure, temperature, ramping and time) proved necessary to avoid device or glass cracks (above 3.5 bar), dye or electrolyte degradation (above 90–100 °C) and incomplete polymerization (less than 2 h processing time). This challenging work demonstrated how a well-established and industrially relevant process could be adapted to the production of a DSSP of significant surface. Then, in the final fabrication step, the edge of the panel was sealed with silicone glue and a metal frame (Figures 2,h and Figure S4) to give the finished product.

2.3 Modules and panel performance

2.3.1 Transparent photovoltaic assessment

Light transmittance, i.e. transparency (AVT), is a physical property of a material that quantifies the amount of light allowed to pass through it without interruption [29,80]. AVT is a mandatory assessment for windows industry to evaluate the transparency level of the transparent PV technology [18,35]. The transparency of the module aperture area on the entire visible range was calculated to be 35.7% (see Equations (S1) and (S2) in the Supporting Information) by considering the transparency of the different sections of the module (sealant, 69.9% on 73.4 cm^2; cells, 27.6% on 222 cm^2; grids, 0% on 20 cm^2) [57,71]. The value is higher compared to the reported literature about DSSC modules [3,53] and perfectly in agreement with BIPV needs [10,18,21,23,24,81]. Besides AVT, the color rendering index (CRI) is an important parameter for building interior space comfort [10,82]. It describes how accurately the color of an object is rendered through a transparent medium [10,35,82–84]. The module active area has *x,y* chromaticity coordinates of 0.454 and 0.339 in the CIE1931 diagram [35,84,85]. In this case, the CRI value is equal to 22.1%, as calculated according to

previous studies [84–86]. Considering the CRI value of the different sections of the module (sealant, 91%; cells, 22.1%; grids, 0%), the CRI of the module aperture area is 36.7%.

Traverse *et al.* introduced the light utilization efficiency (LUE = PCE × AVT) to compare different technologies against theoretical limits and represents an overall (aesthetic and electrical) system efficiency [10,18]. We got a LUE value of 1.8% and 1.0% on active and aperture area, respectively. The values are sufficient to self-power low-power mobile electronic devices and smart windows or complement passive window coatings or smart window technologies [18].

2.3.2 Module testing

Since each string is composed of three modules connected in series (voltages of the modules are summed), it is important to choose modules with comparable currents, because the worst module will drive the string performance (Figure S5). In the following step, the strings are connected in parallel (currents of the strings are summed) to form a panel, so the worst voltage string defines the voltage of the panel. Therefore, during devices sorting, modules in the same string must have comparable currents and the sum of the V_{oc} in each string must be similar (Figure S5). The described procedure guarantees to obtain balanced strings and panel.

A total of 20 modules were assembled during two working days, providing very similar performances in terms of average PCE (4.34% *vs* 4.19%), Isc (203 mA *vs* 205.8 mA), Voc (9.1 V *vs* 8.9 V) and FF (52% *vs* 50.7%), testifying the repeatability of the fabrication process (Figure 3 and Table 2).

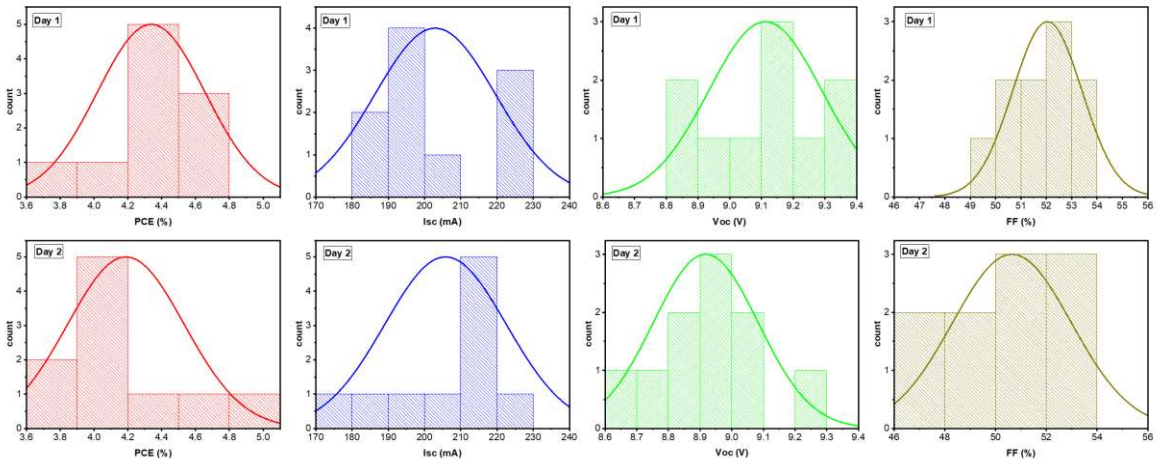

Figure 3. Electrical parameters distribution (histograms are fitted with a Gaussian distribution) of the 20 modules fabricated along two days (10 per day).

Table 2. Average values and standard deviation of the electrical parameters of the 20 modules fabricated in two different days.

	PCE (%)	Isc (mA)	Voc (V)	FF (%)
Day 1	4.34±0.32	203±16.7	9.1±0.2	52±1.4
Day 2	4.19±0.36	205.8±16.8	8.9±0.2	50.7±2.3

The average Voc of the modules (9 V) corresponds to a cell voltage (module voltage/number of cell) of 0.75 V, that is in agreement with the Voc of a DSSC realized with the same materials [71]. The maximum module efficiency recorded was 4.9% with a Voc just below 9 V (Figure 4).

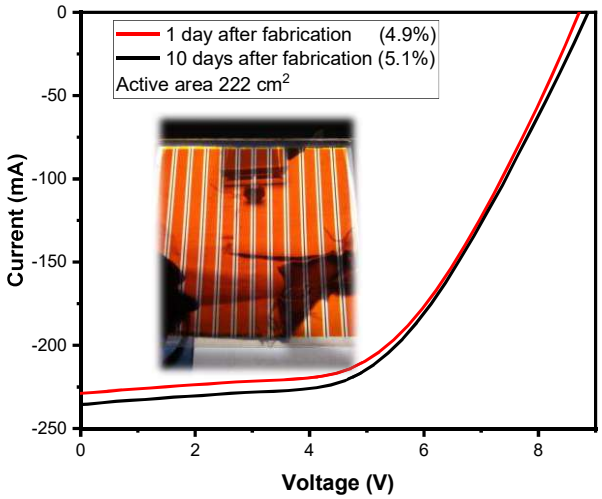

Figure 4. *I/V* plot of the best module.

After ten days from the module assembling, the module efficiency increased till 5.1%. The improvement is related to the penetration of the electrolyte in the TiO_2 matrix, as mentioned below in the discussion on the thermal resistance tests (see Section 2.4). As expected, the FF (54%) is comparable to the value (53%) reached by large area cells (3.6 cm^2) fabricated with the same materials [54], because the cells width and the distance between the end of the cell and the collecting grid/bus bar are comparable between the two devices. The efficiency value decreased when moving from 0.5 to 3.6 and to 222 cm^2, since the resistive losses of the TCO are directly proportional to the width of the cell and the distance between the cells in case of a module [41]. EIS analysis reported for the large area cells revealed low charge transfer resistance at TiO_2/dye/electrolyte interface and high electron lifetime in case of the TTZ5 dye [54]. The latter explains the high Voc obtained with the modules in this work.

2.3.3 Panel testing

We measured the PV properties of the panel (60° tilted respect to the ground) in outdoor conditions at different hours on 1st of June 2021, on the roof of the CNR Research Area in Sesto Fiorentino (Italy) (Table 3). The incident sun power was assessed based on the data provided by the meteorological station of CNR-IBE, located on the roof of the same building where the measurements were made. The weather station setup is available online [87].

Table 3. Electrical parameters of the DSSP at different sun power and related temperatures. Panel tilt 60°; active area 0.2 m^2.

CEST	Sun irradiance (W/m^2)	Temperature (°C)	P_{max} (W)	Isc (mA)	Voc (V)	PCE (%)
12.30	940	25.0°C	3.37	350.11	25.88	1.80
15.00	870	27.0°C	3.75	409.16	26.50	2.16
16.00	730	27.2°C	3.86	416.03	26.42	2.65
17.00	730	26.8°C	3.57	383.94	26.35	2.49

The highest efficiency (2.65%) was recorded at low irradiation intensities (730 W/m^2), because in such conditions the diffusion of redox species in the electrolyte becomes a less limiting factor compared to high irradiation intensities [16]. The panel voltage was about 26.5 V, which corresponds to the parallel connection of three strings formed by three series-connected modules with about 9 V each (Figure S5).

2.4 Stability tests

Stability and durable lifetime are fundamental aspects to be addressed in a DSSC technology upscaling route [44]. Reliable DSSC modules need to show a lifetime ranging from 5 years (low-cost electronic applications) to 20 years (power-plant or BIPV). There are intrinsic and extrinsic degradation mechanisms related to dye, electrolyte, platinum and titania, but a large area device should be stable at molecular, cell and module level [47]. Temperatures above 50 °C have a detrimental effect on DSSC devices durability for different reasons: dye dissolution in the electrolyte [78]; dye desorption from TiO_2 layer [88]; irreversible loss of I_2 and I_3^- [89]; electrolyte

leakage and degradation of the CE [42,88,90,91]. Moreover, sealant failure and delamination further boost the degradation mechanisms.

Since specific certification protocols for DSSC technology have not been identified, ISOS protocols, IEC 61215, JIS C8938 and JIS C8991 can be adopted [3,61,92]. We performed an ISOS-D-2 test (dry conditions at 85 °C) in oven at Voc and an ISOS-L-1 test (light soaking at MPP-Maximum Power Point, see Experimental Section) on four modules (two for each test) not used for the panel (Figure 5).

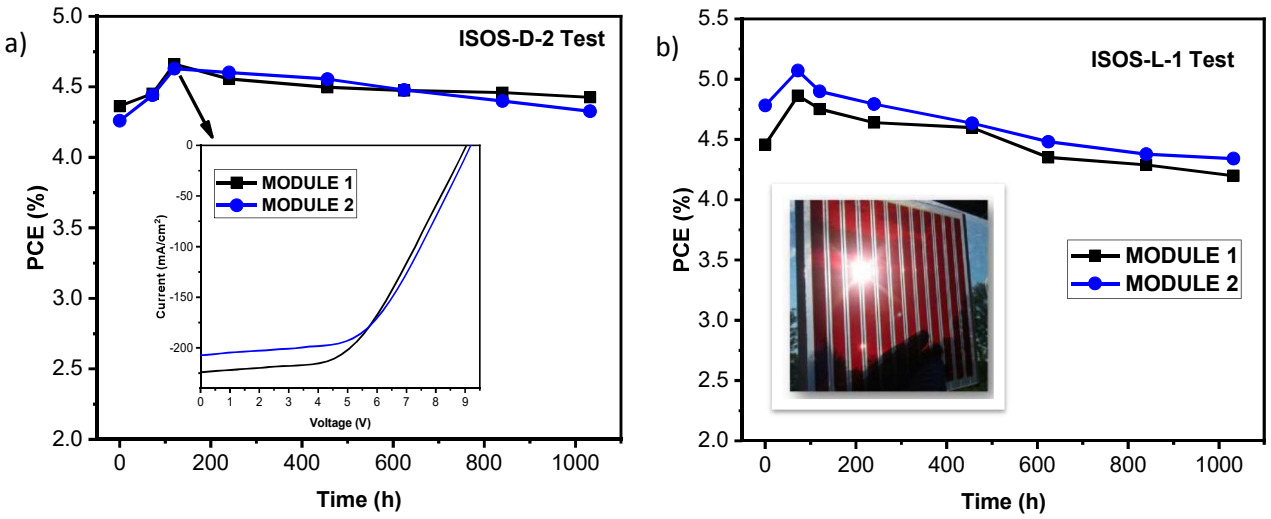

Figure 5. a) ISOS-D-2 and b) ISOS-L-1 stability test of four different DSSMs.

After 120 h thermal stress, the modules increased the efficiency about 8% compared to the initial value (Figure 5a). Such performance improvement is a phenomenon already discussed in the literature [93,94]: the temperature reduces the electrolyte viscosity that helps the penetration in the mesoporous TiO_2. This improves the ionic diffusion and a fast dye chemical reduction, boosting FF and current. After 1000 h, the efficiency was still about 3% higher than the initial value, although it was reduced by about 6% respect to the highest value after 120 h. Since the results are comparable with the same thermal test on cells [54], we can confirm that module connections, sealing and fabrication process do not add any stability issue [95]. Moreover, we noticed no electrolyte leakage, grids corrosion, empty liquid electrolyte zones and moiré patterns on the sealing part (Figure S6). The thermal expansion of the glass substrates and electrolytes, and the sealant strain are the main issues related to the mechanical sturdiness of DSSMs [42,44,52,76,91]. Researchers designed and adopted a wide cell width (18 mm) to reduce the difference in thermal expansion [52,76]. Here, we obtained stable DSSMs with a cell width of 10.25 mm by the optimized process engineering. In Figure S2, we show how the gap between the CE and the PE did not change considerably after the

thermal stress at 85 °C. We tested two modules under continuous and constant illumination at 1 Sun and MPP (Figure 5b). The PCE progressively increased during the first 70 h up to 5.1%, then it started to drop, albeit with losses smaller than 10% and 15% (after 1000 h) compared to the initial and champion value, respectively. As for the ISOS-D-2 test, the modules did not present any issue related to sealing failures or grids corrosion.

3. Conclusion

The architectural versatility and the very good low-light performance highlight the full potential of DSSC technology in the BIPV industry [96]. Besides DSSM efficiency, transmittance should be carefully considered in BIPV sector, as the solar transmission also influences the building energy consumption. The materials composing the cell play a key role both in terms of efficiency and transparency. Since the window transparency influences the lighting condition of the interior and the energy consumption, thick TiO_2 layers provide higher PCEs compared to thin layers, but without improving the overall efficiency of the building [9]. The most suitable dye for outdoor installation must be resistant to temperatures above 50 °C to avoid dye dissolution in the electrolyte and dye desorption from TiO_2 layer. In this study, we focused on the design and manufacturing of modules, strings and panels by considering the three main features of a potential BIPV installation: efficiency, transparency and durability of the devices. The best efficiency on active area is 5.1% (aspect ratio above 70%), the transparency is 35.7% (LUE above 1.8%) and the modules are stable at 85 °C (ISOS-D-2 test) and under light soaking (ISOS-L-1 test) for more than 1000 h, thanks to the gap uniformity between PE and CE and the reliable sealing process. After sorting 20 highly reproducible modules by considering the series connection to build a string and the parallel connection to realize a panel, we laminated a 0.2 m^2 panel according to an industrially compatible method. The panel has a maximum efficiency of 2.7% in outdoor conditions with 60° tilt angle. If compared to the reported literature in the introduction, the devices have similar dimensions and exhibit comparable efficiency to our previous work, but they featured an in-house developed organic dye and did not present any change in the used materials respect to the stability test performed. Moreover, the AVT is higher than any previous reported semi-transparent DSSM. We also showed the fabrication, the design and the aspect ratio details of the devices, from module to panel. Finally, we reported stability tests of semi-transparent modules, filling a literature gap. The reported procedure can pave the way for a scalable, systematic and stable module/panel fabrication process on large scale.

4. Experimental Section

The full fabrication process took place in ambient air.

Module Fabrication: FTO (fluorinated tin oxide)-covered glass sheets (Pilkington TEC7, 2.2 mm thick) were cut in a size of 19.2×20 cm^2 and bevelled on the edge. Then, the substrates were patterned to form 12 series connected cells by a nanosecond raster scanning laser (λ=1064 nm, Nd:YVO_4) and cleaned with soap, acetone and ethanol, successively. This step was crucial to have good adhesion of the subsequently deposed materials and to avoid contamination. A silver ink (Chimet, 3700 80%) was deposited by a semi-automatic screen-printer (Baccini-Applied Materials) with 77.48 mesh to realize the conductor grids and the bus-bars. The substrates were dried at 120°C for 30 min (Lenton WHT6/60 oven) before the deposition by screen-printing technique of TiO_2 (GreatCell Solar 18-nrt with 43.80 mesh) and of Pt (3D Nano Pt-106 with 100.40 mesh) inks on PEs and on CEs, respectively. The PEs were inserted in a box for 5 min to guarantee the material levelling and smoothness of the layer. Then PEs were sintered at 500 °C for 30 min (2.5 h ramping) and CEs were fired at 480 °C for 30 min (2 h ramping). Ten PEs at a time were heated at 100 °C for 15 min, dipped vertically in the dye solution (0.2 mM TTZ5 in THF) while still hot, and kept for 15 h, typically overnight, to let the dye molecules be absorbed onto the mesoporous TiO_2 surface. After soaking, PEs were rinsed with THF and Ethanol and dried in air. Both absorption and cleaning processes were carried out in a laboratory room where the UV component of the light was filtered. A Bynel™ thermoplastic gasket (80 μm thick) was shaped according to the module layout by a cutting plotter (Smallone V). Then, the gasket was stuck without melting on the CE by a thermal press (Memo 50) at 1.6 bar/125 °C for 60 sec. PE and CE were sealed together and aligned to series connecting the grids, and the thermoplastic foil became transparent after the polymerization (1.8 bar/165 °C for 70 sec). The spacing of the electrodes was about 60 μm. The HSE electrolyte (triiodide/iodide redox couple in 3-methoxypropionitrile, with inorganic/organic iodide salt and an imidazole derivative as additives) from Great Cell Solar was injected in 10 modules by the designed vacuum back filling system through the 60 μm slits (one per cell) shaped in the gasket when preparing the thermoplastic foil. Then, the slits were sealed by positioning under the press (1.8 bar/180 °C for 80 sec) the edge of the module to avoid thermal and pressure overexposure of the polymer in the main part of the device.

Panel fabrication: After module sorting, 3 modules were connected in series by overlapping the bus-bars to realize a string. Three strings were connected in parallel with a conductive tin ribbon soldered on the bus bars. Then, two cables were applied on the positive and negative contact. The panel (58.3 × 60 cm^2) was sandwiched in between two 4 mm thick tempered glass and two 1.52 mm

thick PVB (polyvinyl butyral) foils and then inserted in a silicone bag under vacuum. The bag was placed in an industrial autoclave (Bombi) at 3.3 bar/100 °C (40 min/60 min ramping) for few minutes. The full process lasted 2 h. Then, the edge of the panel was sealed with silicone glue and a metal frame (final dimensions 59 cm × 61 cm × 1.8 cm).

Characterization: The film profiles were measured using a profilometer (DEKTAK 150, Veeco Instruments Inc.). The procedure to measure the gap between the two assembled electrodes was as follows. We marked 9 points on the two substrates (Figure S2): the bottom substrate with a scribe parallel to the silver fingers and the top substrate with a scribe orthogonal to the previous one to form a cross. With the confocal microscope (OLS-4000 system, Olympus) we detected the focal planes in correspondence of the scribe in the top substrate and in the bottom substrate. Then, we calculated the distance of the two scribes (i.e. gap/thickness of the chamber) along the z-axis measuring the difference between the absolute values of the two focal planes. The optical analysis related to dye concentration, AVT and CRI was performed with a UV-vis spectrometer (UV-2550, Shimadzu). AVT and CRI measurements correspond to a complete device assessment and were determined according to the Supporting Information and to the literature [80,84–86]. The photovoltaic characteristics of the modules were measured with a class B sun simulator (KHS, Solar Constant 1200) at AM 1.5 1000W/m^2 calibrated with a SKS 1110 sensor (Skye Instruments Ltd.); the system was equipped with a 2612 source meter (Keithley Instruments Inc.) and a LabVIEW interface. During the measurement a UV filter was placed on top of the module. The light soaker (Arkeo CICCI Research) is a low mismatch cool white LED based system (400-750 nm). A LabViEW/Python based code manages the J/V and MPP tracking state. A standard perturb-and-observe tracking algorithm was selected for the devices. The photovoltaic characterization of the panel was performed in outdoor conditions on the 1st of June 2021 in Sesto Fiorentino (Italy, exact coordinates: N 43° 49’ 07’’, E 11° 12’ 04’’), on a mostly sunny day. J/V curves were measured with a B2901A digital source meter (Keysight Technologies). The incident sun power was assessed based on the data provided by the meteorological station of CNR-IBE, located on the roof of the same building where the measurements were made [87].

Supporting Information

Supporting Information is available from the Wiley Online Library

Acknowledgements

The authors thank RoberGlass S.r.l. (Calci, Italy) for assistance in panel lamination. P.M. and L.V. would like to thank Ms. Maryam Esmaeilzadeh (University of Rome "Tor Vergata") for lab assistance and Dr. Diego Di Girolamo (University of Rome "Tor Vergata") for fruitful discussion. The authors thank Mr. Carlo Bartoli (CNR-ICCOM) for the fabrication of the metallic panel support frame (tilt angle 60°C). Financial support by the Ministry of Economic Development (MISE) within the "Research on the Electric System – High Efficiency Photovoltaics" project (project n. PTR_19_21_CNR_PRG_1), as well as by Tuscany Region within the "SELFIE - System of multi-layer advanced elements based on innovative surfaces and nanostructured materials for sustainable and energy efficient buildings" research project (FAR-FAS Call 2014), is gratefully acknowledged. L.V. was supported by the European Union's Horizon 2020 Framework Program for funding Research and Innovation under grant agreement no. 826013 (IMPRESSIVE).

References

[1] M. Grätzel, *J. Photochem. Photobiol. C Photochem. Rev.* **2003**, *4*, 145.

[2] M. Grätzel, *Nature* **2001**, *414*, 338.

[3] L. Vesce, A. Guidobaldi, P. Mariani, A. Di Carlo, M. L. Parisi, S. Maranghi, R. Basosi, in *World Sci. Ref. Hybrid Mater.*, **2019**, pp. 423–485.

[4] A. B. Muñoz-García, I. Benesperi, G. Boschloo, J. J. Concepcion, J. H. Delcamp, E. A. Gibson, G. J. Meyer, M. Pavone, H. Pettersson, A. Hagfeldt, M. Freitag, *Chem. Soc. Rev.* **2021**, *50*, 12450.

[5] M. A. Green, E. D. Dunlop, J. Hohl-Ebinger, M. Yoshita, N. Kopidakis, X. Hao, *Prog. Photovoltaics Res. Appl.* **2020**, *28*, 629.

[6] O. Almora, D. Baran, G. C. Bazan, C. Berger, C. I. Cabrera, K. R. Catchpole, S. Erten-Ela, F.

Guo, J. Hauch, A. W. Y. Ho-Baillie, T. J. Jacobsson, R. A. J. Janssen, T. Kirchartz, N. Kopidakis, Y. Li, M. A. Loi, R. R. Lunt, X. Mathew, M. D. McGehee, J. Min, D. B. Mitzi, M. K. Nazeeruddin, J. Nelson, A. F. Nogueira, U. W. Paetzold, N. G. Park, B. P. Rand, U. Rau, H. J. Snaith, E. Unger, L. Vaillant-Roca, H. L. Yip, C. J. Brabec, *Adv. Energy Mater.* **2021**, *11*, 2102526.

[7] A. Fakharuddin, R. Jose, T. M. Brown, F. Fabregat-Santiago, J. Bisquert, *Energy Environ. Sci.* **2014**, *7*, 3952.

[8] G. Tulloch, *J. Photochem. Photobiol. A Chem.* **2004**, *164*, 209.

[9] S. Yoon, S. Tak, J. Kim, Y. Jun, K. Kang, J. Park, *Build. Environ.* **2011**, *46*, 1899.

[10] F. Grifoni, M. Bonomo, W. Naim, N. Barbero, T. Alnasser, I. Dzeba, M. Giordano, A. Tsaturyan, M. Urbani, T. Torres, C. Barolo, F. Sauvage, *Adv. Energy Mater.* **2021**, *11*, 2101598.

[11] H. Otaka, M. Kira, K. Yano, S. Ito, H. Mitekura, T. Kawata, F. Matsui, *J. Photochem. Photobiol. A Chem.* **2004**, *164*, 67.

[12] P. Selvaraj, H. Baig, T. K. Mallick, J. Siviter, A. Montecucco, W. Li, M. Paul, T. Sweet, M. Gao, A. R. Knox, S. Sundaram, *Sol. Energy Mater. Sol. Cells* **2018**, *175*, 29.

[13] Luigi Vesce and Riccardo Riccitelli, *Prog. Photovoltaics Res. Appl.* **2012**, *20*, 960.

[14] S. Khanna, S. Sundaram, K. S. Reddy, T. K. Mallick, *Appl. Therm. Eng.* **2017**, *127*, 559.

[15] L. Dominici, L. Vesce, D. Colonna, F. Michelotti, T. M. Brown, A. Reale, A. Di Carlo, *Appl. Phys. Lett.* **2010**, *96*, 13302.

[16] A. Hagfeldt, G. Boschloo, L. Sun, L. Kloo, H. Pettersson, *Chem. Rev.* **2010**, *110*, 6595.

[17] M. L. Parisi, S. Maranghi, L. Vesce, A. Sinicropi, A. Di Carlo, R. Basosi, *Renew. Sustain.*

Energy Rev. **2020**, *121*, 109703.

[18] C. J. Traverse, R. Pandey, M. C. Barr, R. R. Lunt, *Nat. Energy* **2017**, *2*, 849.

[19] A. Cannavale, U. Ayr, F. Martellotta, *Energy Procedia* **2017**, *126*, 636.

[20] X. Cao, X. Dai, J. Liu, *Energy Build.* **2016**, *128*, 198.

[21] F. Martellotta, A. Cannavale, U. Ayr, *Energy Procedia* **2017**, *126*, 219.

[22] L. Vesce, M. Stefanelli, F. Matteocci, L. A. Castriotta, E. Lamanna, J. Herterich, F. Di Giacomo, M. Kohlstadt, U. Wurfel, A. Di Carlo, *12th AEIT Int. Annu. Conf. AEIT 2020* **2020**, DOI 10.23919/AEIT50178.2020.9241096.

[23] T. Miyazaki, A. Akisawa, T. Kashiwagi, *Renew. Energy* **2005**, *30*, 281.

[24] P. Boyce, N. Eklund, S. Mangum, C. Saalfield, L. Tang, *Int. J. Light. Res. Technol.* **1995**, *27*, 145.

[25] C. Hachem, A. Athienitis, P. Fazio, *Energy Procedia* **2014**, *57*, 1815.

[26] S. De Sousa, C. Olivier, L. Ducasse, G. Le Bourdon, L. Hirsch, T. Toupance *ChemSusChem* **2013**, *6*, 993.

[27] S. Ito, S. M. Zakeeruddin, R. Humphry-Baker, P. Liska, R. Charvet, P. Comte, M. K. Nazeeruddin, P. Péchy, M. Takata, H. Miura, S. Uchida, M. Grätzel, *Adv. Mater.* **2006**, *18*, 1202.

[28] G. Calogero, J. Barichello, I. Citro, P. Mariani, L. Vesce, A. Bartolotta, A. Di Carlo, G. Di Marco, *Dye. Pigment.* **2018**, *155*, 75.

[29] A. A. F. Husain, W. Z. W. Hasan, S. Shafie, M. N. Hamidon, S. S. Pandey, *Renew. Sustain. Energy Rev.* **2018**, *94*, 779.

[30] P. Selvaraj, H. Baig, T. K. Mallick, J. Siviter, A. Montecucco, W. Li, M. Paul, T. Sweet, M.

Gao, A. R. Knox, S. Sundaram, *Sol. Energy Mater. Sol. Cells* **2018**, *175*, 29.

[31] J. Barichello, P. Mariani, F. Matteocci, L. Vesce, A. Reale, A. Di Carlo, M. Lanza, G. Di Marco, S. Polizzi, G. Calogero, *Nanomaterials* **2022**, *12*, 267.

[32] S. Hore, C. Vetter, R. Kern, H. Smit, A. Hinsch, *Sol. Energy Mater. Sol. Cells* **2006**, *90*, 1176.

[33] H. Arakawa, T. Yamaguchi, A. Takeuchi, S. Agatsuma, *Conf. Rec. 2006 IEEE 4th World Conf. Photovolt. Energy Conversion, WCPEC-4* **2006**, *1*, 36.

[34] Q. Huaulmé, V. M. Mwalukuku, D. Joly, J. Liotier, Y. Kervella, P. Maldivi, S. Narbey, F. Oswald, A. J. Riquelme, J. A. Anta, R. Demadrille, *Nat. Energy* **2020**, *5*, 468.

[35] W. Naim, V. Novelli, I. Nikolinakos, N. Barbero, I. Dzeba, F. Grifoni, Y. Ren, T. Alnasser, A. Velardo, R. Borrelli, S. Haacke, S. M. Zakeeruddin, M. Graetzel, C. Barolo, F. Sauvage, *JACS Au* **2021**, *1*, 409.

[36] L. Han, A. Fukui, Y. Chiba, A. Islam, R. Komiya, N. Fuke, N. Koide, R. Yamanaka, M. Shimizu, *Appl. Phys. Lett.* **2009**, *94*, 013305.

[37] X. C. Zhang, J., Lin, H., Li, J. B., Li, X. & Zhao, *Key Eng. Mater.* **2010**, *434*.

[38] L. Dai, S., Wang, K., Weng, J., Sui, Y., Huang, Y., Xiao, s., Chen, S., Hu, L., Kong, F., Pan, X., Shi, C., and Guo, *Sol. Energy Mater. Sol. Cells* **2005**, *85*, 447.

[39] L. Vesce, R. Riccitelli, G. Mincuzzi, A. Orabona, G. Soscia, T. M. Brown, A. Di Carlo, A. Reale, *IEEE J. Photovoltaics* **2013**, *3*, 1004.

[40] A. Fukui, N. Fuke, R. Komiya, N. Koide, R. Yamanaka, H. Katayama, L. Han, *Appl. Phys. Express* **2009**, *2*, 82202.

[41] E. Giordano, Fabrizio Guidobaldi, Andrea Petrolati, L. Vesce, R. Riccitelli, A. Reale, T.

Brown, A. Di Carlo, *Prog. Photovoltaics Res. Appl.* **2012**, *21*, 1653.

[42] R. Sastrawan, J. Beier, U. Belledin, S. Hemming, A. Hinsch, R. Kern, C. Vetter, F. M. Petrat, A. Prodi-Schwab, P. Lechner, W. Hoffmann, *Prog. Photovoltaics Res. Appl.* **2006**, *14*, 697.

[43] L. Vesce, M. Stefanelli, L. A. Castriotta, A. Hadipour, S. Lammar, B. Yang, J. Suo, T. Aernouts, A. Hagfeldt, A. Di Carlo, *Sol. RRL* **2022**, DOI https://doi.org/10.1002/solr.202101095.

[44] S. Castro-Hermosa, S. K. Yadav, L. Vesce, A. Guidobaldi, A. Reale, A. Di Carlo, T. M. Brown, *J. Phys. D. Appl. Phys.* **2017**, *50*, 33001.

[45] L. Vesce, M. Stefanelli, J. P. Herterich, L. A. Castriotta, M. Kohlstädt, U. Würfel, A. Di Carlo, *Sol. RRL* **2021**, *5*, 2100073.

[46] L. A. Castriotta, F. Matteocci, L. Vesce, L. Cinà, A. Agresti, S. Pescetelli, A. Ronconi, M. Löffler, M. M. Stylianakis, F. Di Giacomo, P. Mariani, M. Stefanelli, E. M. Speller, A. Alfano, B. Paci, A. Generosi, F. Di Fonzo, A. Petrozza, B. Rellinghaus, E. Kymakis, A. Di Carlo, *ACS Appl. Mater. Interfaces* **2021**, *13*, 11741.

[47] J. B. Baxter, *J. Vac. Sci. Technol. A Vacuum, Surfaces, Film.* **2012**, *30*, 020801.

[48] M. Späth, P. M. Sommeling, J. A. M. Van Roosmalen, H. J. P. Smit, N. P. G. Van Der Burg, D. R. Mahieu, N. J. Bakker, J. M. Kroon, *Prog. Photovoltaics Res. Appl.* **2003**, *11*, 207.

[49] Y. Takeda, N. Kato, K. Higuchi, A. Takeichi, T. Motohiro, S. Fukumoto, T. Sano, T. Toyoda, *Sol. Energy Mater. Sol. Cells* **2009**, *93*, 808.

[50] D. Joly, L. Pellejà, S. Narbey, F. Oswald, T. Meyer, Y. Kervella, P. Maldivi, J. N. Clifford, E. Palomares, R. Demadrille, *Energy Environ. Sci.* **2015**, *8*, 2010.

[51] H. M. Lee, J. H. Yoon, *Appl. Energy* **2018**, *225*, 1013.

[52] H. Kim, J. Jo, G. Lee, M. Shin, J. C. Lee, *Sol. Energy* **2017**, *155*, 585.

[53] M. Godfroy, J. Liotier, V. M. Mwalukuku, D. Joly, Q. Huaulmé, L. Cabau, C. Aumaitre, Y. Kervella, S. Narbey, F. Oswald, E. Palomares, C. A. González Flores, G. Oskam, R. Demadrille, *Sustain. Energy Fuels* **2021**, *5*, 144.

[54] A. Dessì, M. Calamante, A. Mordini, M. Peruzzini, A. Sinicropi, R. Basosi, F. Fabrizi De Biani, M. Taddei, D. Colonna, A. Di Carlo, G. Reginato, L. Zani, *RSC Adv.* **2015**, *5*, 32657.

[55] A. Dessì, M. Calamante, A. Mordini, M. Peruzzini, A. Sinicropi, R. Basosi, F. de Biani, M. Taddei, D. Colonna, A. Di Carlo, G. Reginato, L. Zani, *Chem. Commun.* **2014**, *50*, 13952.

[56] M. L. Parisi, A. Dessì, L. Zani, S. Maranghi, S. Mohammadpourasl, M. Calamante, A. Mordini, R. Basosi, G. Reginato, A. Sinicropi, *Front. Chem.* **2020**, *8*, 214.

[57] J. Barichello, L. Vesce, P. Mariani, E. Leonardi, R. Braglia, A. Di Carlo, A. Canini, A. Reale, *Energies* **2021**, *14*, 6393.

[58] P. Mariani, L. Vesce, A. Di Carlo, *Semicond. Sci. Technol.* **2015**, *30*, 104003.

[59] P. Mariani, L. Vesce, A. Di Carlo, *IEEE 4th Int. Forum Res. Technol. Soc. Ind. RTSI 2018 - Proc.* **2018**, DOI 10.1109/RTSI.2018.8548439.

[60] P. Mariani, A. Agresti, L. Vesce, S. Pescetelli, A. L. Palma, F. Tomarchio, P. Karagiannidis, A. C. Ferrari, A. Di Carlo, *ACS Appl. Energy Mater.* **2021**, *4*, 98.

[61] M. V. Khenkin, E. A. Katz, A. Abate, G. Bardizza, J. J. Berry, C. Brabec, F. Brunetti, V. Bulović, Q. Burlingame, A. Di Carlo, R. Cheacharoen, Y. B. Cheng, A. Colsmann, S. Cros, K. Domanski, M. Dusza, C. J. Fell, S. R. Forrest, Y. Galagan, D. Di Girolamo, M. Grätzel, A. Hagfeldt, E. von Hauff, H. Hoppe, J. Kettle, H. Köbler, M. S. Leite, S. (Frank) Liu, Y. L. Loo, J. M. Luther, C. Q. Ma, M. Madsen, M. Manceau, M. Matheron, M. McGehee, R. Meitzner, M. K. Nazeeruddin, A. F. Nogueira, Ç. Odabaşı, A. Osherov, N. G. Park, M. O.

Reese, F. De Rossi, M. Saliba, U. S. Schubert, H. J. Snaith, S. D. Stranks, W. Tress, P. A. Troshin, V. Turkovic, S. Veenstra, I. Visoly-Fisher, A. Walsh, T. Watson, H. Xie, R. Yıldırım, S. M. Zakeeruddin, K. Zhu, M. Lira-Cantu, *Nat. Energy* **2020**, *5*, 35.

[62] M. O. Reese, S. A. Gevorgyan, M. Jørgensen, E. Bundgaard, S. R. Kurtz, D. S. Ginley, D. C. Olson, M. T. Lloyd, P. Morvillo, E. A. Katz, A. Elschner, O. Haillant, T. R. Currier, V. Shrotriya, M. Hermenau, M. Riede, K. R. Kirov, G. Trimmel, T. Rath, O. Inganäs, F. Zhang, M. Andersson, K. Tvingstedt, M. Lira-Cantu, D. Laird, C. McGuiness, S. Gowrisanker, M. Pannone, M. Xiao, J. Hauch, R. Steim, D. M. Delongchamp, R. Rösch, H. Hoppe, N. Espinosa, A. Urbina, G. Yaman-Uzunoglu, J. B. Bonekamp, A. J. J. M. Van Breemen, C. Girotto, E. Voroshazi, F. C. Krebs, *Sol. Energy Mater. Sol. Cells* **2011**, *95*, 1253.

[63] T. N. Matsui H, Okada K, Kawashima T, Ezure T, K. R. and W. M, *J. Photochem. Photobiol. A* **2004**, *164*, 129.

[64] N. Matsui, H., Okada, K., Kitamura, T., and Tanabe, *Sol. Energy Mater. Sol. Cells* **2009**, *93*, 1110.

[65] R. Goldstein, J. R., Breen, B., Yakupov, I., Hodesh, R., and Paz, *Photovoltaic Cell*, **2008**, WO 2008/139479 A2.

[66] K. Okada, H. Matsui, T. Kawashima, T. Ezure, N. Tanabe, *J. Photochem. Photobiol. A Chem.* **2004**, *164*, 193.

[67] J. A. Hopkins, G. Phani, I. L. Skryabin, *Methods to Implement Interconnects in Multi-Cell Regenerative Photovoltaic Photoelectrochemical Devices*, **2003**, US 6,555,741 B1.

[68] G. Tulloch, I. L. Skryabin, *Photoelectrochemical Device*, **2004**, WO 2004/100196 A1.

[69] S. Venkatesan, W. H. Lin, H. Teng, Y. L. Lee, *ACS Appl. Mater. Interfaces* **2019**, *11*, 42780.

[70] S. Ito, S. M. Zakeeruddin, P. Comte, P. Liska, D. Kuang, M. Grätzel, *Nat. Photonics* **2008**, *2*,

693.

[71] A. Dessì, M. Calamante, A. Sinicropi, M. L. Parisi, L. Vesce, P. Mariani, B. Taheri, M. Ciocca, A. Di Carlo, L. Zani, A. Mordini, G. Reginato, *Sustain. Energy Fuels* **2020**, *4*, 2309.

[72] G. Mincuzzi, L. Vesce, M. Schulz-Ruhtenberg, E. Gehlen, A. Reale, A. Di Carlo, T. M. Brown, *Adv. Energy Mater.* **2014**, *4*, 1400421.

[73] G. Mincuzzi, M. Schulz-Ruhtenberg, L. Vesce, A. Reale, A. Di Carlo, A. Gillner, T. M. Brown, *Prog. Photovoltaics Res. Appl.* **2014**, *22*, 308.

[74] G. Mincuzzi, L. Vesce, M. Liberatore, A. Reale, A. Di Carlo, T. M. Brown, *IEEE Trans. Electron Devices* **2011**, *58*, 3179.

[75] S. G. Hashmi, M. Özkan, J. Halme, S. M. Zakeeruddin, J. Paltakari, M. Grätzel, P. D. Lund, *Energy Environ. Sci.* **2016**, *9*, 2453.

[76] C. Han, S. Il Park, *2014 15th Int. Conf. Therm. Mech. Multi-Physics Simul. Exp. Microelectron. Microsystems, EuroSimE 2014* **2014**, 1.

[77] E. Figgemeier, A. Hagfeldt, *Int. J. Photoenergy* **2004**, *6*, 127.

[78] M. I. Asghar, K. Miettunen, J. Halme, P. Vahermaa, M. Toivola, K. Aitola, P. Lund, *Energy Environ. Sci.* **2010**, *3*, 418.

[79] S. Ito, T. N. Murakami, P. Comte, P. Liska, C. Grätzel, M. K. Nazeeruddin, M. Grätzel, *Thin Solid Films* **2008**, *516*, 4613.

[80] E. U. Finlayson, D. K. Arasteh, C. Huizenga, M. D. Rubin, M. S. Reilly, *Window 4.0: Documentation of Calculation Properties*, Lawrence Berkeley Lab., Enermodal Eng. Inc., **1993**.

[81] S. B. Chae YT, Kim J, Park H, *Appl. Energy* **2014**, *129*, 217.

[82] A. Roy, A. Ghosh, S. Bhandari, P. Selvaraj, S. Sundaram, T. K. Mallick, *J. Phys. Chem. C* **2019**, *123*, 23834.

[83] A. Ghosh, S. Sundaram, T. K. Mallick, *Renew. Energy* **2019**, *131*, 730.

[84] A. Ghosh, P. Selvaraj, S. Sundaram, T. K. Mallick, *Sol. Energy* **2018**, *163*, 537.

[85] P. K. Kaiser, *Commission Internationale de l'Eclairage. CIE 1988, 2° Spectral Luminous Efficiency Function for Photopic Vision, CIE 086-1990*, **1990**.

[86] C. Yang, D. Liu, M. Bates, M. C. Barr, R. R. Lunt, *Joule* **2019**, *3*, 1803.

[87] "Weather station setup," can be found under http://www.lamma.rete.toscana.it/en/meteo/osservazioni-e-dati/dati-stazioni/2395conf, (accessed June 2021)

[88] T. Lund, P. T. Nguyen, H. M. Tran, P. Pechy, S. M. Zakeeruddin, M. Grätzel, *Sol. Energy* **2014**, *110*, 96.

[89] P. M. Sommeling, M. Späth, H. J. P. Smit, N. J. Bakker, J. M. Kroon, *J. Photochem. Photobiol. A Chem.* **2004**, *164*, 137.

[90] I. Lee, S. Hwang, H. Kim, *Sol. Energy Mater. Sol. Cells* **2011**, *95*, 315.

[91] A. G. Kontos, T. Stergiopoulos, V. Likodimos, D. Milliken, H. Desilvestro, G. Tulloch, P. Falaras, *J. Phys. Chem. C* **2013**, *117*, 8636.

[92] P. Kumar, C. Bilen, B. Vaughan, X. Zhou, P. C. Dastoor, W. J. Belcher, *Sol. Energy Mater. Sol. Cells* **2016**, *149*, 179.

[93] A. Hinsch, J. M. Kroon, R. Kern, I. Uhlendorf, J. Holzbock, A. Meyer, J. Ferber, *Prog. Photovoltaics Res. Appl.* **2001**, *9*, 425.

[94] A. B. Djurišić, F. Liu, A. M. C. Ng, Q. Dong, M. K. Wong, A. Ng, C. Surya, *Phys. Status*

Solidi - Rapid Res. Lett. **2016**, *10*, 281.

[95] C. H. Kwak, J. H. Baeg, I. M. Yang, K. Giribabu, S. Lee, Y. S. Huh, *Sol. Energy* **2016**, *130*, 244.

[96] J. Gong, K. Sumathy, Q. Qiao, Z. Zhou, *Renew. Sustain. Energy Rev.* **2017**, *68*, 234.

TOC Graphic

Process Engineering of Semi-transparent DSSC Modules and Panel Incorporating an Organic Sensitizer

L. Vesce, P. Mariani, M. Calamante, A. Dessì, A. Mordini, L. Zani, A. Di Carlo**

We demonstrate a reliable and reproducible method to fabricate under ambient air conditions several large-area dye-sensitized solar modules (400 cm^2) and a panel (0.2 m^2) containing an organic dye. The finest module efficiency is more than 5% (35.7% AVT) with thermal (ISOS-D-2) and light stability (ISOS-L-1). An industrially-compatible process was adopted to laminate the panel, which showed an outdoor efficiency of 2.7%.